ROYAL SOCIETY OF CHEMISTRY

PAPER

Check for updates

A material catalogue with glass-like thermal conductivity mediated by crystallographic occupancy for thermoelectric application†

Zihang Liu, ‡[a] Wenhao Zhang,‡[ab] Weihong Gao[a] and Takao Mori ★[ab]

Discovering materials with intrinsically low lattice thermal conductivity κ_{lat} is an important route for achieving high thermoelectric performance. In reality, the conventional synthetic approach, however, relies on trial and error. Herein, we proposed a new crystallographic parameter, namely the site occupancy factor, as an effective indicator to identify a material catalogue with low κ_{lat}. Taking Cu_6Te_3S, in which some Cu atoms show partial occupancy, as the representative sample, it was found that this compound exhibited ultralow κ_{lat} with weak temperature dependence from 5 K to 350 K. The appearance of a boson peak and unusual two-level tunneling states in the heat capacity measurement revealed the low-lying optical modes and dynamic diffusion disorder, respectively. This glass-like thermal property in a crystalline material arose from the combination of the anharmonic and anisotropic vibration of the Cu atom, the ionic bond feature around the Cu atom, and the global weak bonding, confirmed by the calculated phonon dispersion, electron localization function, and potential energy curves. Utilizing the proposed indicator of partial occupancy, we searched in the Crystallography Open Database for further potential candidate materials with low κ_{lat}. As a further test of the efficacy of this strategy, two unearthed compounds were synthesized and both were indeed found to exhibit very low κ_{lat}, around 0.6 W m^{-1} K^{-1} at 300 K. Our work explored the close relationship between crystallography and thermal property in crystalline materials and revealed the impact of partial occupancy in complex lattice dynamics, opening up new avenues towards discovering materials with low κ_{lat}.

Broader context

The thermoelectric effect enables the direct conversion of heat into electricity and *vice versa*, which has received intensive interest for powering IoT devices and cooling applications. Discovering materials with an intrinsically low lattice thermal conductivity κ_{lat} is an important route for decoupling these interrelated thermoelectric parameters and therefore achieving high thermoelectric performance. The conventional synthetic approach used long-term has been based largely on laboratory trial and error, or complex quantum calculations. In this study, we proposed a new crystallographic parameter, namely the site occupancy factor, as an effective indicator to identify a material catalogue with low κ_{lat} using the REST-API framework. In a representative material, Cu_6Te_3S, which contains Cu with partial occupancy, an amorphous thermal conductivity was observed and, more importantly, the thermoelectric performance can be further enhanced by Ag alloying on the Cu site. The corresponding phonon mechanism of low κ_{lat} was attributed to the anharmonic and anisotropic vibration of the Cu atom, the ionic bond feature around the Cu atom, and the global weak bonding. Our study offers fresh insights into discovering materials with low κ_{lat} for thermoelectric applications.

Introduction

The ability to tune the thermal conductivity is vital in diverse technological applications. One important aspect is to discover or design inorganic materials with a low thermal conductivity as potential thermal barrier coatings and thermoelectric materials.[1,2] The thermoelectric effect enables the direct conversion of heat into electricity and *vice versa*, which has received interest for powering Internet of Things (IoT) devices and cooling applications.[3–5] The dimensionless thermoelectric

[a] *WPI Center for Materials Nanoarchitectonics (WPI-MANA), National Institute for Materials Science (NIMS), Namiki 1-1, Tsukuba 305-0044, Japan.*
E-mail: MORI.Takao@nims.go.jp

[b] *Graduate School of Pure and Applied Sciences, University of Tsukuba, Tennodai 1-1-1, Tsukuba 305-8671, Japan.*

† Electronic supplementary information (ESI) available. See DOI: 10.1039/d1ee00738f
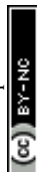‡ These authors contributed equally to this work.

figure of merit (ZT), defined as $ZT = (S^2\sigma/\kappa_{tot})T$, dominates the conversion efficiency, where S, σ, κ_{tot}, and T are the Seebeck coefficient, the electrical conductivity, the total thermal conductivity (including lattice thermal conductivity κ_{lat} and electronic thermal conductivity κ_{ele}) and the absolute temperature, respectively. The parameter κ_{ele} usually follows the Wiedemann–Franz law, and is linearly proportional to σ and T. Considering the intertwined or contradicted thermoelectric parameters (S, σ, and κ_{ele}),[6] optimizing the charge carrier concentration[7–9] or suppressing κ_{lat} through nano–microstructural engineering[10–15] is the common method to increase ZT.

Alternatively, discovering materials with an intrinsically low κ_{lat} is another important route for achieving high ZT in thermoelectrics.[16–18] Nearly all good thermoelectric materials are heavily doped semiconductors. The transport of thermal energy in crystalline semiconductors is predominantly by atomic vibrations, which can be quantized by the quasiparticle 'phonon'. The parameter κ_{lat} can be approximately estimated based on the simple kinetic theory:

$$\kappa_{lat} = \frac{1}{3}C_v v_p l_p \qquad (1)$$

where C_v is the specific heat capacity at constant volume, ν_p is the phonon group velocity, and l_p is the phonon mean free path (MFP). Typical crystal features, such as the heavy element constituent, complex structure, or a large number of atoms in the unit cell,[19–21] are valid empirical rules for discovering materials with low κ_{lat}, due to the lower ν_p and short MFP of phonons. It should be emphasized that in boride compounds, in the context of disorder, partial occupancy of rare earth sites is assumed to contribute to the observed glass-like thermal property,[19,22,23] but the related mechanisms have not been explicitly analyzed in detail. Recently, the large suppression of thermal conductivity from lone pair coordination,[24,25] resonant bonding,[26–28] bonding heterogeneity,[29,30] rattling atoms,[31–33] strong anharmonicity,[34,35] and liquid-like behavior[36–40] has been identified. The microscopic understanding of these phenomena requires time-consuming theoretical investigation on lattice dynamics, making it difficult to use them as a guide in the search for low thermal conductivity materials in advance.

The conventional synthetic approach to discovering materials with low κ_{lat} values has for a long time been based on significant laboratory trial and error. Some recently developed methods, including high-throughput computation,[41] inverse design approach,[42] and machine learning[43] have accelerated the discovery process, all of which, however, rely on complex quantum calculations and/or models. Herein, we report, for the first time, that the crystallographic site occupancy can be used to enable the simple and efficient search for materials with low κ_{lat}. According to the theory of harmonic lattice vibration, l_p would be infinite in a perfect lattice but becomes finite once the periodicity is broken. Thus, the reduction in translational symmetry will lead to a reduced κ_{lat}. Partial occupancy is a source of such reduction in periodicity, which can be easily checked by looking at crystal structures, therefore serving as the first indicator of lattice thermal conductivity. For Cu_6Te_3S,

which contains Cu atoms showing partial occupancy, the observed temperature dependence and the magnitude of κ_{lat}, as well as low-temperature heat capacity measurements, were similar to those of amorphous materials, and are closely related to the partial occupancy. Density-functional theory (DFT) calculations reveal that the corresponding microscopic mechanism originates from the anharmonic and anisotropic vibration of the Cu atom, the ionic bond feature around the Cu atom, and the global weak bonding, which unveils the unusual phonon conduction of crystalized compounds with partial occupancy.

Results and discussion

Pristine Cu_6Te_3S exhibits a phase transition around 404 K from the low-temperature α phase to the high-temperature β phase, displayed in Fig. 1a. Both α-Cu_6Te_3S and β-Cu_6Te_3S crystallize in the cubic system with different space groups of $P2_13$ and $P\bar{4}3n$,[44] respectively. The high-temperature phase can be seen as a Cu-filled Cr_3Si structure type and the low-temperature cell is 8 times bigger. One unusual feature in these two crystal structures is the distinct site occupancy factor (sof) of the Cu atoms. In α-Cu_6Te_3S, 4 out of 11 Cu sites are fully occupied while the other Cu atoms show partial occupancy. By contrast, all Cu atoms in β-Cu_6Te_3S are fully disordered with lower partial occupancy. In crystallography, there are two kinds of partial occupancy with a sof value of less than unity in terms of an average unit cell: there are mixtures of atoms that share the same crystallographic site (substitutional disorder) or there are mixtures that contain fewer atoms than there are symmetry equivalent sites to occupy. The latter is the one occurring in our currently investigated system of Cu_6Te_3S, signifying the spatial fluctuations of Cu atoms at some Wyckoff positions. If there is no strict description, partial occupancy in the following context means the latter condition. It should be mentioned that filler atoms in skutterudite also show the partial occupancy feature,[45] which, however, has received little attention about its effect on lowering the κ_{lat}. Fig. 1b shows that the powder X-ray diffraction (XRD) refinement result exhibits a reasonable fit with the model of collection code 427 560 in the Inorganic Crystal Structure Database (ICSD) and no strong peaks of the impurity phase are observed within the detection limit. The microscale homogeneity was further confirmed by scanning electron microscopy (SEM) and energy dispersive spectrometry (EDS) composition mapping analysis (Fig. S1, ESI†). The composition analysis shows that the atomic percentage of Cu, Te, and S elements is 60.57, 29.62, and 9.81, respectively, which is close to the nominal composition. The thermogravimetry (TG) curve for the synthesized Cu_6Te_3S ingot from 373 K to 773 K under a N_2 flow atmosphere confirms that the weight drop is almost negligible over the entire temperature range (Fig. S2, ESI†). Besides, the sintering temperature of Cu_6Te_3S is at a relatively low temperature (723 K), which seems not to be high enough for inducing the sulfur loss. Overall, the effect of sulfur loss on the thermoelectric properties of Cu_6Te_3S can be neglected, although sulfur loss sometimes occurs in
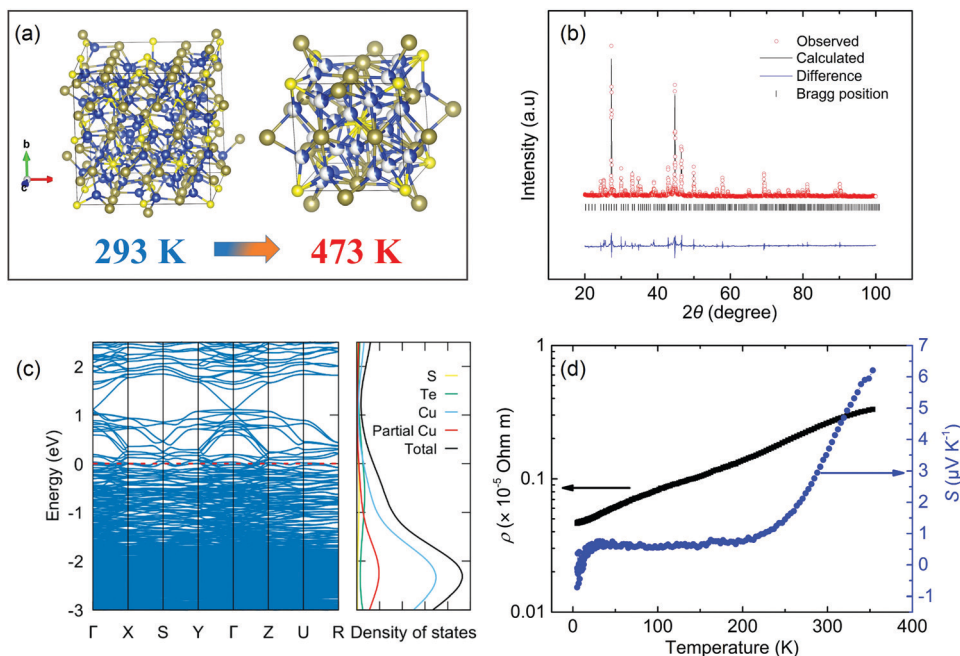
Fig. 1 Structure and electrical transport properties of Cu_6Te_3S. (a) Crystal structure; (b) XRD refinement result; (c) electronic band structure and DOS; and (d) temperature-dependent electrical conductivity ρ and Seebeck coefficient S from 5 K to 350 K.

Cu–chalcogen compounds during sintering, leading to the introduction of disorder and a low κ_{lat}.[46,47]

For our DFT calculation, a cubic unit cell containing 160 atoms is used. The minimum $2 \times 2 \times 2$ supercell would contain more than 1000 atoms, which becomes impractical for DFT calculation. We generate the fixed structure by filling the partial occupancy site but keep the symmetry of the resulting cell as the space group $P2_12_12_1$ for calculation efficiency. According to the crystal symmetry and those crystallographic sites with partial occupancy, the configuration of partial occupancy that needs to be considered is reduced. In the end, 4 of them with the smallest ground state energy for the phonon calculation are chosen. The detailed calculation method in terms of the partial-occupancy-structure was displayed in the ESI.† The results of electronic and phononic structures are almost identical, suggesting that the specific choice of Cu site does not have a big impact on the physical properties. We show one of the band structures in Fig. 1c while the others are displayed in Fig. S3 (ESI†). No band gap is found in its electronic band structure with a finite DOS at the Fermi energy, indicating a metallic character. The larger density of states just below the Fermi level leads to p-type conduction. The measured low-temperature electrical resistivity ρ and Seebeck coefficient S in Fig. 1d also support this conclusion of metallic conduction. The temperature dependence of ρ is positive from 5 K to 350 K, in which the relatively small residual resistivity ratio (RRR ρ_{300K}/ρ_{5K} = 5.7) and the high ρ at 300 K $\sim$2.6 μΩ m are an indicator of poor metallic behavior. The positive S is near constant at low temperature but changes to a linearly positive temperature dependence from 200 K to 350 K.

After subtracting the κ_{ele} component based on the Wiedemann–Franz law, it was found that Cu_6Te_3S exhibits an extremely low κ_{lat} over the entire measured temperature range in Fig. 2a.

For example, the peak κ_{lat} value is less than 0.7 W m^{-1} K^{-1}, lower than those of typical low thermal conductivity materials such as In_4Se_3,[48] Zn_4Sb_3,[49] and α-$MgAgSb$,[29] while the room temperature κ_{lat} value is around 0.3 W m^{-1} K^{-1} which is even lower than those of amorphous SiO_2.[50] The weak temperature dependence resembles glass-like behavior. The slow increase in κ_{lat} at low temperature is mainly due to the increase in phonon heat capacity and, based on eqn (1), we can deduce a weakly temperature-dependent l_p at low temperature. The disappearance of the peak-shape dependence in $\kappa_{lat}(T)$ also occurs in some crystalline materials with a strong structural disorder, including $(KBr)_{1-x}(KCN)_x$,[51] complex boride compounds,[19,21,22] skutterudites and clathrates with a filler[32,52] as well as ionic semiconductors.[36,53] This similarity in magnitude and temperature dependence between Cu_6Te_3S and amorphous materials is ascribed to the Cu atom partial occupancy, as well as the resulting atomic-level dynamic heterogeneity, the ionic bond feature around the Cu atom, and the global weak bonding, revealed by the following DFT calculations.

The low-temperature heat capacity C_p was measured to probe the related phonon contribution mechanism, which was present as C_p/T^3 as a function of T over the T range from 2 K to 20 K in Fig. 2b. The complete C_p data from 2 K to 350 K are displayed in Fig. S4 (ESI†). A hump from 10 K to 20 K, referred to as the "boson peak," is observed, which is related to the excess phonon density of states (DOS) resulting from these low-lying optical modes.[54] In addition to amorphous solids, this behavior has recently been reported in some crystalline solids, such as clathrates,[32] Cu_3SbSe_3,[30] α-$MgAgSb$,[29] and $CsSnBrI_2$.[28] More importantly, there is a clear upturn below 3 K in Cu_6Te_3S, which did not occur in these abovementioned systems but which has been observed previously in rare earth borides.[22,55] This can be explained by the two-level tunneling
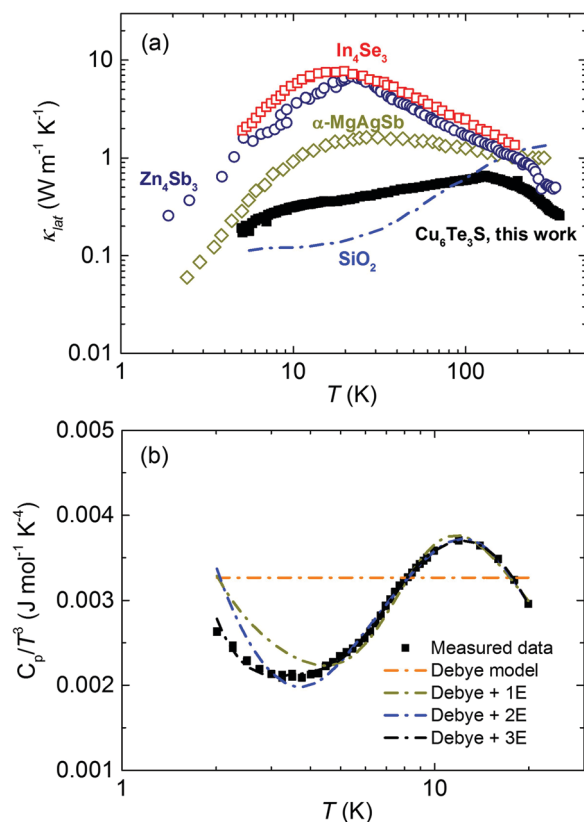
This journal is © The Royal Society of Chemistry 2021

Energy Environ. Sci., 2021, **14**, 3579–3587 | **3581**

Fig. 2 Thermal properties of Cu_6Te_3S. (a) Temperature dependent lattice thermal conductivity κ_{lat} of Cu_6Te_3S from 5 K to 350 K, in comparison with other typical materials with a low thermal conductivity, including In_4Se_3,[48] Zn_4Sb_3,[49] α-MgAgSb,[29] Cu_2Se,[53] and amorphous SiO_2.[50] (b) Temperature-dependent heat capacity C_p, depicted as C_p/T^3 as a function of T. The dashed lines are fitting results based on the Debye model, Debye-1 Einstein oscillator model (Debye + 1E), Debye-2 Einstein oscillator model (Debye + 2E), and Debye-3 Einstein oscillator model (Debye + 3E).

states in amorphous solids,[56] corresponding to two neighboring equilibrium positions. As pointed out by Phillips, "we can say that tunneling states will occur in materials with an open structure".[56] This unusual phenomenon in Cu_6Te_3S should be ascribed to the unique crystallographic occupancy, in which the existence of atomic partial occupancy results in Cu atoms tunneling among several possible crystallographic sites with low formation energy. Therefore, the migration of Cu may also occur in Cu_6Te_3S, especially at high temperature, and has commonly occurred in Cu–chalcogen compounds, like Cu_2Se and $Cu_{12+x}Sb_4S_{13}$.[36,57] In general, the atomic partial occupancy, as the fundamental mechanism, leads to the possible atomic migration and complex lattice dynamics.

The experimental C_p/T^3 data show a strong deviation from the classical Debye model dependence and, therefore, the Debye–Einstein model with a different number of oscillators was utilized, as shown in the following equation:

$$C_p/T = \delta + \beta T^2 + \sum_{i=1}^{n} A_i (\Theta_{Ei}) 2 \cdot \left(T^2\right)^{-3/2} \cdot \frac{e^{\Theta_{Ei}/T}}{\left(e^{\Theta_{Ei}/T} - 1\right)^2} \quad (2)$$

where the first term is the electron contribution in which δ is the Sommerfeld constant, the second term is the Debye lattice contribution, and the final term is related to the Einstein oscillator at a specific Einstein temperature Θ_{Ei}. Herein, until introducing three Einstein oscillators, the data show perfect fitting. The fitting parameters for these three models were given in Tables S1 and S2 (ESI†). The existence of the Einstein oscillator indicates the strong coupling between acoustic phonons and low-frequency optical phonons,[58] which would effectively affect the contribution of acoustic phonons to heat conduction. Besides, the obtained Debye temperature θ_D is about 147 K, lower than that of other typical low thermal conductivity materials, such as α-MgAgSb (201 K)[29,59] and Cu_2Se (295 K).[53] It signifies the extremely weak chemical bonding, namely the low ν_p and slow phonon propagation in Cu_6Te_3S. This can be further confirmed by the experimental sound velocity measurements (the longitudinal sound velocity $\nu_l \approx 2648$ m s^{-1} and the transverse sound velocity $\nu_t \approx 1323$ m s^{-1} at 300 K). According to eqn (1), the calculated l_p at 300 K is about 3 Å, close to the interatomic bonding length, which indicates that it is approaching the minimum thermal conductivity.

The calculated phonon dispersion in Fig. 3a shows the extremely soft acoustic phonons with an ultralow cutoff frequency around 0.6 THz at the Brillouin zone boundary, comparable to these materials with intrinsically low thermal conductivity, e.g., Ag_9GaSe_6 (0.54 THz),[38] MgAgSb (0.6 THz),[29,59] and PbTe (0.78 THz).[26] This corresponding origin is due to the combination of weak chemical bonding and a large primitive cell ~ 3176.1 Å^3. The former leads to the low ν_p defined as the
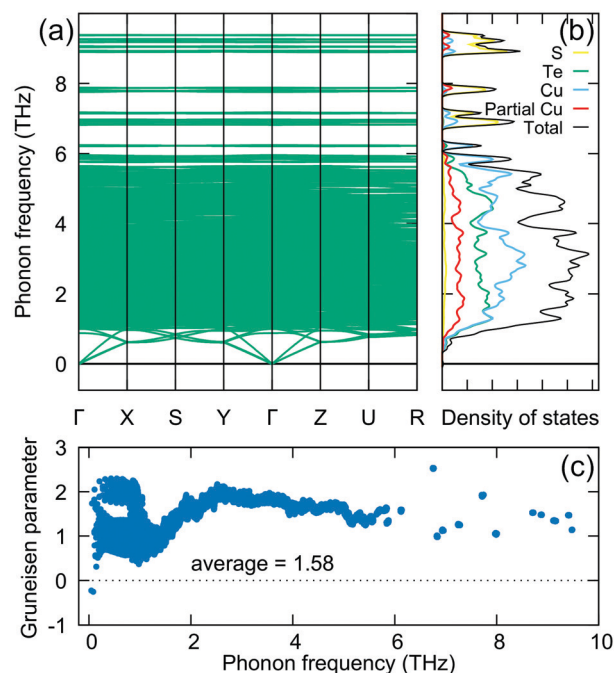

Fig. 3 The calculated lattice dynamics and ELF plot in Cu_6Te_3S. (a) Phonon dispersion, (b) the projected phonon DOS, and (c) the Grüneisen parameter.

3582 | *Energy Environ. Sci.*, 2021, **14**, 3579–3587

This journal is © The Royal Society of Chemistry 2021

slope of the acoustic dispersion relation, while the latter restricts the zone boundary of the first Brillouin zone. It is known that the low cutoff frequency is directly associated with the low κ_{lat} according to the Debye model prediction. Besides, the hybridization between acoustic phonons and low-frequency optical phonons can be also observed. In one of the calculated configurations, we even found some low-lying optical phonons, solely involving the partially occupied Cu atom (Fig. S5, ESI†), leading to the anticrossing behavior.[58] These calculations are supportive of the observation of the boson peak in our C_p analysis.

The corresponding projected phonon DOS in Fig. 3b reveals that the main contribution of low-energy phonons (<2 THz) originates from the Cu atom, including fixed Cu atoms and partial-occupancy Cu atoms. It indicates that the Cu atom is responsible for the complex lattice dynamics of Cu_6Te_3S. The calculated average Grüneisen parameter γ, characterizing the strength of the anharmonicity of the lattice vibration, is about 1.58, close to the obtained value based on the sound velocity of ~ 2.0, demonstrating the relatively strong lattice anharmonicity in Cu_6Te_3S. The typical expression of Umklapp scattering that dominates the high-temperature phonon scattering in solids is shown in the following:[20]

$$\kappa_{lat} = \frac{(6\pi^2)^{2/3}}{4\pi^2} \frac{\bar{M}\nu_s^3}{TV^{2/3}\gamma^2} \left(\frac{1}{N^{1/3}}\right) \qquad (3)$$

where $\bar{M}$ is the average atomic mass, ν_s is the average sound velocity, V is the volume per atom, and N is the number of atoms per primitive cell. Together with the low $\nu_s \approx 1484$ m s^{-1} and the large $N \approx 160$, the resulting strong Umklapp scattering in Cu_6Te_3S limits the heat conduction.

To understand the chemical bonding environment in Cu_6Te_3S, we further calculated the electron localization function (ELF) since the ELF is a simple measure of electron localization in an atomic and molecular system.[60] The ELF values are defined between 0 and 1, in which ELF = 1 means the perfect localization and ELF = 0.5 corresponds to the electron gas. From the three-dimensional and the two-dimensional ELFs in Fig. 4a and b, respectively, the following can be learned: (1) the Te atom possesses an asymmetrically distributed electron cloud, with a higher density regime approaching the direction where there is a large interatomic space due to the existence of the Cu atom partial occupancy. (2) The strongly localized electron on the Cu atom illustrates the ionic bond feature while the Te atom with the neighboring Te atom shares electrons as an indication of covalent bonding. The physical binding feature of the Cu atom accounts for the global weak bonding environment in Cu_6Te_3S.

To further gain insight into the lattice anharmonicity and chemical bonding strength in Cu_6Te_3S, the potential energy surface can be a conceptual tool for analysis. The potential energy as a function of displacement in Fig. 5 was calculated on four different crystallographic sites, respectively. Both the Te atom and the S atom show a rather harmonic potential that is also relatively isotropic along the three Cartesian directions. By contrast, a non-parabolicity was observed for the Cu atom,
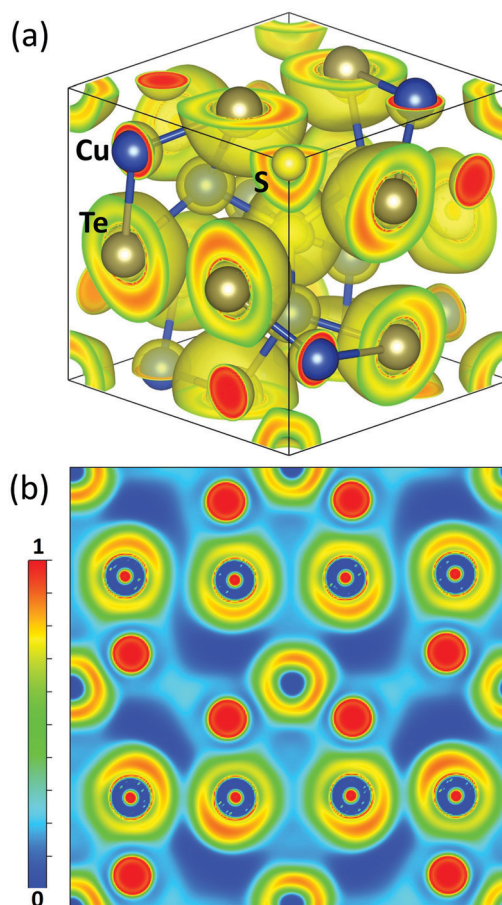

Fig. 4 Calculated ELF plots in Cu_6Te_3S. (a) The three-dimensional ELF, as the 1/8 corner of the unit cell with $0.5 < x, y, z < 1$ and viewed from the [111] direction, and (b) the two-dimensional ELF projected onto the (001) plane.

including the fixed Cu atom and the partial-occupancy Cu atom, indicating the anharmonic feature. Besides, their interatomic force constants (IFCs) are also smaller, especially for the partially occupied Cu site, suggesting loose spring constants of vibration around the equilibrium position and anisotropic behavior. In this scenario, Cu atoms, due to the partial occupancy, do not belong to the static disorder category but show dynamic disorder with anharmonic and anisotropic vibration, which underscores the origin of this unusual glass-like κ_{lat} on the atomic scale.

In addition to this specific example of Cu_6Te_3S, we further search for potential candidates of compounds with partial occupancy in the entirely open-access Crystallography Open Database (COD) via the REpresentational State Transfer (REST) Application Programming Interface (API) approach that offers great convenience, flexibility and scalability for users to access and use data from the targeted database. Detailed information on the REST-API method can be found in the ESI.† To reduce the number of candidates, we only consider binary or ternary compounds containing Te, Se, Sb, Ge, or S elements and we check the structure information from their Crystallographic Information File (CIF) files using the python PyCifRW package.
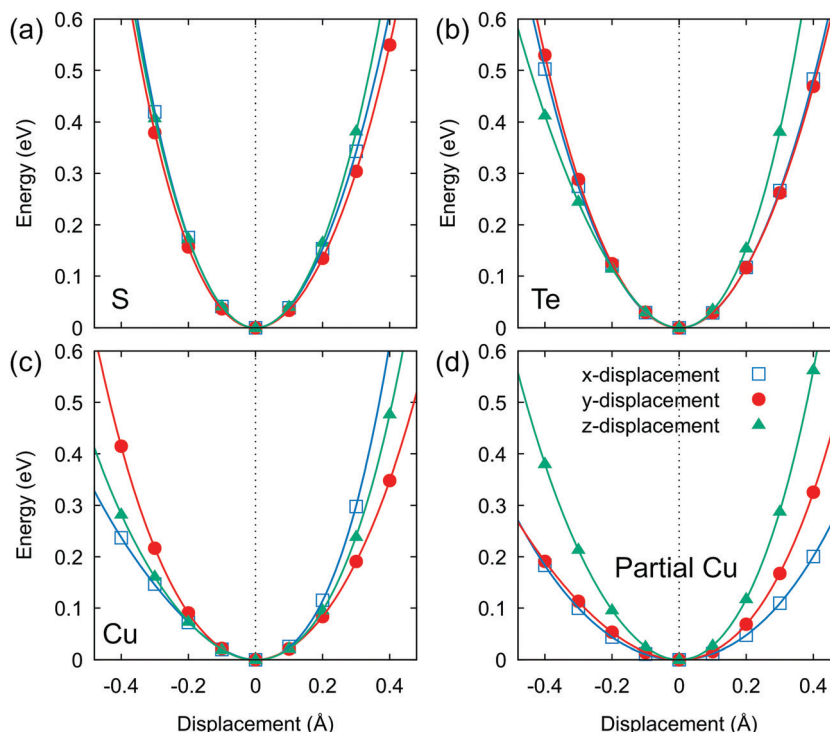
This journal is © The Royal Society of Chemistry 2021

Energy Environ. Sci., 2021, 14, 3579–3587 | 3583

Fig. 5 Calculated potential energy curves as a function of displacement in Cu_6Te_3S along the x, y, and z directions (a, b, and c cell vector), respectively. (a) S atom, (b) Te atom, (c) fixed Cu atom, and (d) Cu atom with partial occupancy.

We selected two compounds (Bi_5CuS_8 and Cr_5Te_8) and experimentally synthesized them, both of which are single phase (Fig. S6, ESI†). Their corresponding crystal structure is given in Fig. S7 (ESI†) where the partial occupancy is shown and highlighted. After measuring their thermoelectric properties (Fig. S8 and S9, ESI†), both of them are found to possess an ultralow κ_{lat} with weak temperature dependence (Fig. 6), where the corresponding room-temperature value is around 0.64 W m^{-1} K^{-1} and 0.55 W m^{-1} K^{-1} for Cr_5Te_8 and Bi_5CuS_8, respectively. It should be mentioned that the relative densities of Cu_6Te_3S, Bi_5CuS_8, and Cr_5Te_8 are above 97% (Table S3, ESI†), which would guarantee that the measured thermoelectric properties,

especially for thermal conduction, are not affected by the pore effect. Besides, the Lorenz number L used in the Wiedemann–Franz law is shown in Fig. S10 (ESI†).

The obtained data in Fig. 7a include 6320 compounds, in which 1587 compounds contain the partial occupancy feature. Combining κ_{lat} data from our current work, and other typical compounds reported with and without partial occupancy, Fig. 7b highlights their anomalously low κ_{lat} values in partially occupied compounds in comparison with common semiconductors,[61] with the x- and y-axes indicating their unit cell volume and average mass per atom, respectively. It should be noted that although compounds with partial occupancy often tend to have a large unit cell volume due to the reduction of translational symmetry, their κ_{lat} values are significantly lower than those of Zintl compounds that possess a complex crystal structure and heavy atomic mass.[62,63]

Table S4 (ESI†) lists the corresponding parameters of these common semiconductors and Zintl compounds, as well as the compounds with partial occupancy of Fig. 7b. Therefore, the most significant discovery is the direct observation of low κ_{lat} in compounds with partial occupancy, demonstrating the close relationship between intrinsic crystal disorder and thermal properties. This new indicator of atom site occupancy, with no need for time-consuming phonon calculations, enables simple and efficient screening to search for new materials with low κ_{lat}.

Despite the intrinsically low κ_{lat} of Cu_6Te_3S, the small S, e.g., 6 μV K^{-1} at 300 K, results in the low thermoelectric performance. The sudden change of thermoelectric properties of
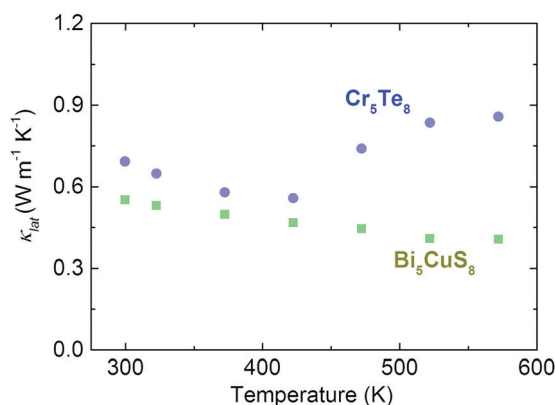

Fig. 6 Temperature dependent lattice thermal conductivity κ_{lat} of Bi_5CuS_8 and Cr_5Te_8.

3584 | *Energy Environ. Sci.*, 2021, **14**, 3579–3587

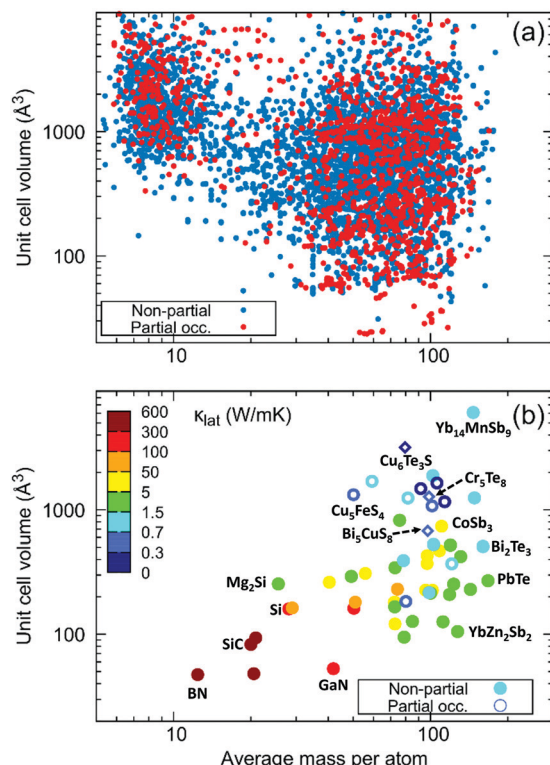This journal is © The Royal Society of Chemistry 2021

Fig. 7 The importance of partial occupancy as a function of unit cell volume and average mass per atom. (a) The obtained database of potential candidates of compounds with partial occupancy; and (b) a comparison of κ_{lat} among common semiconductors (including elements, I–V–VI$_2$, I$_2$–IV–VI$_3$, I$_3$–V–VI$_4$, I–V–VI$_2$, II$_2$–IV, III–V, IV–VI, and V$_3$–VI$_2$ compounds),[61] Zintl compounds[62,63] (including CoSb$_3$, CaZn$_2$Sb$_2$, YbZn$_2$Sb$_2$, Ca$_3$AlSb$_3$, Sr$_3$GaSb$_3$, Yb$_{11}$InSb$_9$, and Yb$_{14}$MnSb$_9$) and compounds with partial occupancy (including Ag$_8$GeTe$_6$,[64] Ba$_8$Ga$_{16}$Ge$_{30}$,[65] Ba$_2$Sb$_2$Se$_5$,[66] Cu$_4$Bi$_4$Se$_9$,[67] Cu$_5$FeS$_4$,[68] Cu$_4$Sn$_7$S$_{16}$,[69] Cu$_2$SnSe$_4$,[70] Ge$_1$Sb$_4$Te$_7$,[71] and Zn$_8$Sb$_7$[72] as well as Cu$_6$Te$_3$S, Bi$_5$CuS$_8$ and Cr$_5$Te$_8$. Only some important compounds are named in Fig. 7b.

Cu_6Te_3S around 440 K was due to the phase transition, which was confirmed by the differential scanning calorimetry (DSC) analysis (Fig. S11, ESI†). The peak value turns out to be about 439 K, consistent with our thermoelectric properties measurements. Ag alloying on the Cu site was further used to optimize the electrical transport properties. It has been reported that the cation vacancy formation energy can be tuned in $(Cu, Ag)_2Te$,[73,74] in which Cu_2Te possesses the lowest formation energy, probably due to the small Cu atomic radius. Here a similar tendency is also observed that Ag alloying in Cu_6Te_3S leads to a significantly increased ρ (Fig. 8a), in agreement with Ag alloying in Cu_2Te.[73] Specifically, the room-temperature ρ value of $Cu_4Ag_2Te_3S$ is two orders-of-magnitude higher than that of pristine Cu_6Te_3S. Besides, the temperature dependency changes from the metallic type to the semiconductor type as well. Simultaneously, a remarkable enhancement of S is observed after Ag alloying (Fig. 8b), with the maximum room-temperature value surpassing 200 μV K^{-1}. Thanks to the increased ρ, κ_{tot} is obviously reduced (Fig. 8c), where the room-temperature value is about 0.3 W m^{-1} K^{-1}. It should be noted that the small discrepancy in S (and κ_{tot})

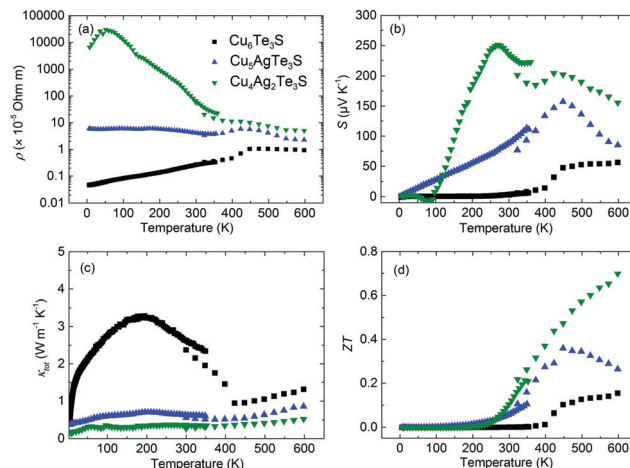Fig. 8 Temperature dependent thermoelectric properties of $Cu_{6-x}Ag_xTe_3S$ (x = 0, 1, and 2). (a)–(d) Electrical resistivity ρ, Seebeck coefficient S, total thermal conductivity κ_{tot}, and ZT, respectively.

between ZEM-2 (laser flash) and PPMS data is due to the radiation heat loss during the PPMS measurement. As a result, Ag alloying in Cu_6Te_3S enables a significant improvement of ZT (Fig. 8d), the maximum ZT, to about 0.7 at 600 K, which is comparable to the well-optimized Cu_2Te based materials at the same temperature range.[73]

It is highly possible that other donor dopants, such as divalent ions on the Cu site or halogen ions on the Te/S site, can also be effective for improving the ZT of Cu_6Te_3S. Besides, since Cu_6Te_3S based materials show an extremely low κ_{lat}, increasing the power factor by modulation doping[75] and magnetic effects[76] may be also promising for the overall enhancement of thermoelectric performance.

Conclusions

In conclusion, we provided new insights into the unique chemical bonding and the complex lattice dynamics of Cu_6Te_3S, which contains the Cu atom with partial occupancy, and first proposed the use of crystallographic occupancy for the simple and efficient screening of materials with low κ_{lat}. The low-temperature lattice thermal conductivity and heat capacity results of Cu_6Te_3S resemble the amorphous property. Based on DFT calculations, the corresponding microscopic mechanism originates from the anharmonic and anisotropic vibration of the Cu atom, the ionic bond feature around the Cu atom, and the global weak bonding. The importance of partial occupancy in thermal properties was further confirmed using the REST-API framework in the Crystallography Open Database, from which we identified a potential material catalogue in which compounds with partial occupancy exhibit an anomalously lower κ_{lat} compared with common semiconductors and Zintl compounds. According to the obtained database, another two compounds with partial occupancy, namely Bi_5CuS_8 and Cr_5Te_8, were experimentally synthesized, both of which exhibited a low κ_{lat}, of around 0.6 W m^{-1} K^{-1} at 300 K. More

This journal is © The Royal Society of Chemistry 2021

Energy Environ. Sci., 2021, **14**, 3579–3587 | **3585**

importantly, Ag alloying on the Cu site in Cu_6Te_3S further significantly increased the electrical resistivity and achieved an enhanced ZT, which emphasizes the possibility of optimized performance in these compounds with partial occupancy *via* chemical doping or alloying for thermoelectric applications.

Conflicts of interest

There are no conflicts to declare.

Acknowledgements

Notes and references

1 D. R. Clarke, *Surf. Coat. Technol.*, 2003, **163**, 67–74.
2 J. Mao, Z. H. Liu, J. W. Zhou, H. T. Zhu, Q. Zhang, G. Chen and Z. F. Ren, *Adv. Phys.*, 2018, **67**, 69–147.
3 I. Petsagkourakis, K. Tybrandt, X. Crispin, I. Ohkubo, N. Satoh and T. Mori, *Sci. Technol. Adv. Mater.*, 2018, **19**, 836–862.
4 G. Tan, M. Ohta and M. G. Kanatzidis, *Philos. Trans. R. Soc., A*, 2019, **377**, 20180450.
5 J. Mao, G. Chen and Z. Ren, *Nat. Mater.*, 2021, **20**, 454–461.
6 T. J. Zhu, Y. T. Liu, C. G. Fu, J. P. Heremans, J. G. Snyder and X. B. Zhao, *Adv. Mater.*, 2017, **29**, 1605884.
7 Z. H. Liu, Y. M. Wang, J. Mao, H. Y. Geng, J. Shuai, Y. X. Wang, R. He, W. Cai, J. H. Sui and Z. F. Ren, *Adv. Energy Mater.*, 2016, **6**, 1502269.
8 Z. H. Liu, W. H. Gao, W. H. Zhang, N. Sato, Q. S. Guo and T. Mori, *Adv. Energy Mater.*, 2020, **10**, 2002588.
9 F. Guo, H. Wu, J. Zhu, H. Yao, Y. Zhang, B. Cui, Q. Zhang, B. Yu, S. J. Pennycook, W. Cai, C.-W. Chu and J. Sui, *Proc. Natl. Acad. Sci. U. S. A.*, 2019, **116**, 21998–22003.
10 B. Poudel, Q. Hao, Y. Ma, Y. C. Lan, A. Minnich, B. Yu, X. Yan, D. Z. Wang, A. Muto, D. Vashaee, X. Y. Chen, J. M. Liu, M. S. Dresselhaus, G. Chen and Z. F. Ren, *Science*, 2008, **320**, 634–638.
11 G. Tan, F. Shi, S. Hao, L.-D. Zhao, H. Chi, X. Zhang, C. Uher, C. Wolverton, V. P. Dravid and M. G. Kanatzidis, *Nat. Commun.*, 2016, **7**, 12167.
12 A. U. Khan, K. Kobayashi, D.-M. Tang, Y. Yamauchi, K. Hasegawa, M. Mitome, Y. M. Xue, B. Z. Jiang, K. Tsuchiya, D. Golberg, Y. Bando and T. Mori, *Nano Energy*, 2017, **31**, 152–159.
13 J. Shuai, Y. Sun, X. Tan and T. Mori, *Small*, 2020, 1906921.
14 D. Qin, H. Wu, S. Cai, J. Zhu, B. Cui, L. Yin, H. Qin, W. Shi, Y. Zhang, Q. Zhang, W. Liu, J. Cao, S. J. Pennycook, W. Cai and J. Sui, *Adv. Energy Mater.*, 2019, **9**, 1902435.
15 Z. H. Liu, J. Mao, T.-H. Liu, G. Chen and Z. F. Ren, *MRS Bull.*, 2018, **43**, 181–186.
16 T. Mori, *Small*, 2017, **13**, 1702013.
17 M. K. Jana and K. Biswas, *ACS Energy Lett.*, 2018, **3**, 1315–1324.
18 Y. Xiao and L.-D. Zhao, *Science*, 2020, **367**, 1196–1197.
19 T. Mori, J. Martin and G. Nolas, *J. Appl. Phys.*, 2007, **102**, 073510.
20 E. S. Toberer, A. Zevalkink and G. J. Snyder, *J. Mater. Chem.*, 2011, **21**, 15843–15852.
21 T. Mori, *J. Solid State Chem.*, 2019, **275**, 70–82.
22 D. G. Cahill, H. E. Fischer, S. Watson, R. Pohl and G. Slack, *Phys. Rev. B: Condens. Matter Mater. Phys.*, 1989, **40**, 3254.
23 T. Mori, *Modules, systems, and applications in thermoelectrics*, CRC Press Taylor and Francis, London, 2012, vol. 14.
24 E. J. Skoug and D. T. Morelli, *Phys. Rev. Lett.*, 2011, **107**, 235901.
25 M. D. Nielsen, V. Ozolins and J. P. Heremans, *Energy Environ. Sci.*, 2013, **6**, 570–578.
26 S. Lee, K. Esfarjani, T. F. Luo, J. W. Zhou, Z. T. Tian and G. Chen, *Nat. Commun.*, 2014, **5**, 3525.
27 W. H. Zhang, N. Sato, K. Tobita, K. Kimura and T. Mori, *Chem. Mater.*, 2020, **32**, 5335–5342.
28 H. Xie, S. Hao, J. Bao, T. J. Slade, G. J. Snyder, C. Wolverton and M. G. Kanatzidis, *J. Am. Chem. Soc.*, 2020, **142**, 9553–9563.
29 P. J. Ying, X. Li, Y. C. Wang, J. Yang, C. G. Fu, W. Q. Zhang, X. B. Zhao and T. J. Zhu, *Adv. Funct. Mater.*, 2017, **27**, 1604145.
30 W. Qiu, L. Xi, P. Wei, X. Ke, J. Yang and W. Zhang, *Proc. Natl. Acad. Sci. U. S. A.*, 2014, **111**, 15031–15035.
31 X. Shi, J. Yang, J. R. Salvador, M. F. Chi, J. Y. Cho, H. Wang, S. Q. Bai, J. H. Yang, W. Q. Zhang and L. D. Chen, *J. Am. Chem. Soc.*, 2011, **133**, 7837–7846.
32 T. Takabatake, K. Suekuni, T. Nakayama and E. Kaneshita, *Rev. Mod. Phys.*, 2014, **86**, 669–716.
33 M. Dutta, S. Matteppanavar, M. V. D. Prasad, J. Pandey, A. Warankar, P. Mandal, A. Soni, U. V. Waghmare and K. Biswas, *J. Am. Chem. Soc.*, 2019, **141**, 20293–20299.
34 L.-D. Zhao, S.-H. Lo, Y. S. Zhang, H. Sun, G. J. Tan, C. Uher, C. Wolverton, V. P. Dravid and M. G. Kanatzidis, *Nature*, 2014, **508**, 373–377.
35 J. Hong and O. Delaire, *Mater. Today Phys.*, 2019, **10**, 100093.
36 H. L. Liu, X. Shi, F. F. Xu, L. L. Zhang, W. Q. Zhang, L. D. Chen, Q. Li, C. Uher, T. Day and G. J. Snyder, *Nat. Mater.*, 2012, **11**, 422–425.
37 K. P. Zhao, P. F. Qiu, Q. F. Song, A. B. Blichfeld, E. Eikeland, D. Ren, B. H. Ge, B. B. Iversen, X. Shi and L. D. Chen, *Mater. Today Phys.*, 2017, **1**, 14–23.
38 S. Q. Lin, W. Li, S. S. Li, X. Y. Zhang, Z. W. Chen, Y. D. Xu, Y. Chen and Y. Z. Pei, *Joule*, 2017, **1**, 816–830.
39 J. Zhang, J. Zhu, L. You, K. Guo, Z. Li, W. Lin, J. Huang and J. Luo, *Mater. Today Phys.*, 2019, **10**, 100095.
40 K. Zhao, P. Qiu, X. Shi and L. Chen, *Adv. Funct. Mater.*, 2020, **30**, 1903867.
41 J. Carrete, W. Li, N. Mingo, S. Wang and S. Curtarolo, *Phys. Rev. X*, 2014, **4**, 011019.
42 R. Gautier, X. W. Zhang, L. H. Hu, L. P. Yu, Y. Y. Lin, T. O. Sunde, D. Chon, K. R. Poeppelmeier and A. Zunger, *Nat. Chem.*, 2015, **7**, 308.

3586 | *Energy Environ. Sci.*, 2021, **14**, 3579–3587

This journal is © The Royal Society of Chemistry 2021

43 T. Wang, C. Zhang, H. Snoussi and G. Zhang, *Adv. Funct. Mater.*, 2020, **30**, 1906041.

44 M. Giller, C. Grotz, B. W. Rudyk, A. Mar and T. Nilges, *Z. Kristallogr.*, 2014, **229**, 831–839.

45 G. Nolas, J. Cohn and G. Slack, *Phys. Rev. B: Condens. Matter Mater. Phys.*, 1998, **58**, 164.

46 Y. Kikuchi, Y. Bouyrie, M. Ohta, K. Suekuni, M. Aihara and T. Takabatake, *J. Mater. Chem. A*, 2016, **4**, 15207–15214.

47 K. Suekuni, Y. Shimizu, E. Nishibori, H. Kasai, H. Saito, D. Yoshimoto, K. Hashikuni, Y. Bouyrie, R. Chetty, M. Ohta, E. Guilmeau, T. Takabatake, K. Watanabe and M. Ohtaki, *J. Mater. Chem. A*, 2019, **7**, 228–235.

48 X. Shi, J. Y. Cho, J. R. Salvador, J. Yang and H. Wang, *Appl. Phys. Lett.*, 2010, **96**, 162108.

49 B. L. Pedersen, H. Birkedal, B. B. Iversen, M. Nygren and P. T. Frederiksen, *Appl. Phys. Lett.*, 2006, **89**, 242108.

50 D. G. Cahill, H. E. Fischer, T. Klitsner, E. Swartz and R. Pohl, *J. Vac. Sci. Technol., A*, 1989, **7**, 1259–1266.

51 D. G. Cahill, S. K. Watson and R. O. Pohl, *Phys. Rev. B: Condens. Matter Mater. Phys.*, 1992, **46**, 6131.

52 J. Cohn, G. Nolas, V. Fessatidis, T. Metcalf and G. Slack, *Phys. Rev. Lett.*, 1999, **82**, 779.

53 H. Liu, J. Yang, X. Shi, S. A. Danilkin, D. Yu, C. Wang, W. Zhang and L. Chen, *J. Materiomics*, 2016, **2**, 187–195.

54 M. T. Dove, M. J. Harris, A. C. Hannon, J. M. Parker, I. P. Swainson and M. Gambhir, *Phys. Rev. Lett.*, 1997, **78**, 1070.

55 T. Tanaka, Y. Shi, T. Mori and A. Leithe-Jasper, *J. Solid State Chem.*, 2000, **154**, 54–60.

56 W. Phillips, *J. Low Temp. Phys.*, 1972, **7**, 351–360.

57 P. Vaqueiro, G. Guélou, A. Kaltzoglou, R. I. Smith, T. Barbier, E. Guilmeau and A. V. Powell, *Chem. Mater.*, 2017, **29**, 4080–4090.

58 O. Delaire, J. Ma, K. Marty, A. F. May, M. A. McGuire, M. H. Du, D. J. Singh, A. Podlesnyak, G. Ehlers, M. Lumsden and B. C. Sales, *Nat. Mater.*, 2011, **10**, 614–619.

59 Z. H. Liu, Y. S. Zhang, J. Mao, W. H. Gao, Y. M. Wang, J. Shuai, W. Cai, J. H. Sui and Z. F. Ren, *Acta Mater.*, 2017, **128**, 227–234.

60 A. Savin, R. Nesper, S. Wengert and T. F. Fässler, *Angew. Chem., Int. Ed. Engl.*, 1997, **36**, 1808–1832.

61 O. Madelung, *Semiconductors: Data Handbook*, Springer, Berlin Heidelberg, New York, 2004.

62 E. S. Toberer, A. F. May and G. J. Snyder, *Chem. Mater.*, 2009, **22**, 624–634.

63 J. Shuai, J. Mao, S. W. Song, Q. Y. Zhang, G. Chen and Z. F. Ren, *Mater. Today Phys.*, 2017, **1**, 74–95.

64 A. Charoenphakdee, K. Kurosaki, H. Muta, M. Uno and S. Yamanaka, *Phys. Status Solidi RRL*, 2008, **2**, 65–67.

65 X. Hou, Y. Zhou, L. Wang, W. Zhang, W. Zhang and L. Chen, *J. Alloys Compd.*, 2009, **482**, 544–547.

66 J. Wang, K. Lee and K. Kovnir, *J. Mater. Chem. C*, 2015, **3**, 9811–9818.

67 Y. Jiang, F. Jia, L. Chen and L.-M. Wu, *ACS Appl. Mater. Interfaces*, 2019, **11**, 36616–36625.

68 P. Qiu, T. Zhang, Y. Qiu, X. Shi and L. Chen, *Energy Environ. Sci.*, 2014, **7**, 4000–4006.

69 C. Bourgès, P. Lemoine, O. I. Lebedev, R. Daou, V. Hardy, B. Malaman and E. Guilmeau, *Acta Mater.*, 2015, **97**, 180–190.

70 W. Li, S. Q. Lin, X. Y. Zhang, Z. W. Chen, X. F. Xu and Y. Z. Pei, *Chem. Mater.*, 2016, **28**, 6227–6232.

71 P. Konstantinov, L. Shelimova, E. Avilov, M. Kretova and V. Zemskov, *Inorg. Mater. (Transl. Neorg. Mater.)*, 2001, **37**, 662–668.

72 J. Wang and K. Kovnir, *J. Am. Chem. Soc.*, 2015, **137**, 12474–12477.

73 K. Zhao, K. Liu, Z. Yue, Y. Wang, Q. Song, J. Li, M. Guan, Q. Xu, P. Qiu, H. Zhu, L. Chen and X. Shi, *Adv. Mater.*, 2019, **31**, 1903480.

74 R. Wu, Z. Li, Y. Li, L. You, P. Luo, J. Yang and J. Luo, *J. Materiomics*, 2019, **5**, 489–495.

75 M. Zebarjadi, G. Joshi, G. Zhu, B. Yu, A. Minnich, Y. Lan, X. Wang, M. Dresselhaus, Z. Ren and G. Chen, *Nano Lett.*, 2011, **11**, 2225–2230.

76 J.-B. Vaney, S. A. Yamini, H. Takaki, K. Kobayashi, N. Kobayashi and T. Mori, *Mater. Today Phys.*, 2019, **9**, 100090.

This journal is © The Royal Society of Chemistry 2021

Energy Environ. Sci., 2021, **14**, 3579–3587 | **3587**